



Guided-jet waves generated by an acoustic source in a jet at a Mach number of 0.95

Christophe Bogey

CNRS, Ecole Centrale de Lyon, INSA Lyon, Universite Claude Bernard Lyon I, Laboratoire de Mécanique des Fluides et d'Acoustique, UMR 5509, 69130 Ecully, France

Corresponding author: Christophe Bogey, christophe.bogey@ec-lyon.fr

(Received 5 July 2025; revised 21 October 2025; accepted 2 November 2025)

The guided-jet waves (GJWs) that may be trapped into a jet are investigated by simulating the propagation of the waves generated by an acoustic source on the axis of a jet at a Mach number of 0.95. The flow is modelled as a cylindrical shear layer to avoid reflections in the axial direction. For the source frequencies considered, GJWs belonging to the first two radial GJW axisymmetric modes are observed. They propagate in the upstream or downstream directions, and are entirely or partially contained in the flow, depending on the frequency. Their amplitudes are quantified. In the frequency-wavenumber space, they lie along the GJW dispersion curves predicted using linear-stability analysis. At specific spatial locations, they vary strongly and sharply with the frequency, exhibiting tonal-like peaks near the frequencies of the stationary points in the dispersion curves where the GJWs are standing waves with zero group velocity. Given the flow configuration, these properties can be attributed to propagation effects not requiring axial resonance between upstream- and downstream-travelling waves. Finally, it can be noted that, upstream of the source, outside the jet, the GJW amplitudes fluctuate in a reverse sawtooth manner with very intense peaks up to 30 dB higher than the levels obtained without flow at 10 jet radii from the source, similarly to the GJW footprints in the near-nozzle spectra of highsubsonic jets.

Key words: aeroacoustics, jet noise, shear-flow instability

1. Introduction

Many studies have been carried out on the waves that are essentially contained in the core of jet flows, often referred to as neutral acoustic waves, trapped waves or guidedjet waves (GJWs). As shown by Tam & Hu (1989), these waves have specific dispersion

relations and eigenfunctions and can be classified into modes depending on their radial and azimuthal structures. The GJWs propagating in the upstream direction, in particular, play a key role in resonance phenomena (Edgington-Mitchell 2019). They can close the feedback loops in jets impinging on a plate (Tam & Ahuja 1990; Bogey & Gojon 2017; Varé & Bogey 2022), in jets interacting with an edge (Jordan *et al.* 2018) or a flat plate (Zaman *et al.* 2015; Tam & Chandramouli 2020), in screeching jets (Gojon, Bogey & Mihaescu 2018; Edgington-Mitchell *et al.* 2018) and in supersonic twin jets (Nogueira & Edgington-Mitchell 2021). For non-screeching free jets, they lead to the generation of peaks in the pressure spectra near the nozzle (Suzuki & Colonius 2006; Brès *et al.* 2018; Bogey 2021; Zaman, Fagan & Upadhyay 2022), and in the far field in the upstream direction (Bogey 2022*b*; Zaman, Fagan & Upadhyay 2023). The peaks have a tonal, sawtooth shape for high-subsonic Mach numbers above 0.80, which has been attributed to the establishment of resonance between upstream- and downstream-travelling GJWs (Towne *et al.* 2017; Schmidt *et al.* 2017). Finally, for initially laminar free jets, the GJWs excite the instability waves near the nozzle (Bogey 2022*a*).

The dispersion relations and eigenfunctions of the GJWs are most often determined in the framework of a linear-stability problem using a vortex-sheet model (Tam & Hu 1989). Depending on the position on the dispersion curves, usually represented as functions of axial wavenumber k_z and Strouhal number $St_D = f D/u_i$, where f is the frequency, and D and u_j are the jet diameter and velocity, the group velocities of the waves can be negative or positive, leading to upstream or downstream directions of propagation, or even zero, yielding standing waves. The radial profiles of the GJWs also vary significantly (Tam & Hu 1989; Towne et al. 2017). The waves have a non-negligible support outside the jet near the sonic line $k_z = -\omega/c_0$, where ω is the pulsation and c_0 is the ambient speed of sound, but are fully confined to the jet flow near $k_z = \omega/(u_i - c_0)$. Thus, they can be referred to as free-stream GJWs in the first case and as duct-like GJWs in the second. The predictions of the vortex-sheet model, in terms of GJW dispersion curves and eigenfunctions, agree well with the data from experiments and simulations in most cases. The use of finite-thickness mixing-layer models may, however, be necessary for thick shear layers (Tam & Ahuja 1990; Edgington-Mitchell & Nogueira 2023; Maia, Fiore & Gojon 2024). Moreover, the models mentioned above provide no information on the GJW amplitudes other than the normalised eigenfunction profiles.

On the basis of the above, simulations are performed in the present work to directly compute GJWs in a jet with finite-thickness mixing layer, with the aim of getting access to all their properties including their true, non-normalised amplitudes. The GJWs are investigated by considering them as the result of a problem of acoustic propagation in the presence of a sheared flow. That was previously the case in the simulations of the propagation of random noise fluctuations and of a pressure pulse in a jet flow by Bogey & Gojon (2017) and Bogey (2024), and in the theoretical analyses of the scattering of acoustic waves through single- and double-vortex sheets by Martini, Cavalieri & Jordan (2019) and Nogueira et al. (2024). The study of Nogueira et al. (2024), in particular, demonstrated that the GJWs can result from acoustic waves generated in the core of the flow. These waves were shown to experience internal reflection and transmission from the two shear layers behaving like a soft duct, for a given range of frequencies and wavenumbers, the phase of the reflection coefficient determining the wavenumbers of the GJWs. Transmission of the waves to the outside was also found to be maximum near the sonic line and to rapidly decrease as the waves become subsonic, explaining the formation of partially or fully confined GJW modes.

In this work, a monopolar single-frequency sound source is placed on the axis of a jet to generate axisymmetric GJWs. The jet is modelled as a cylindrical shear layer

to avoid reflections in the axial direction and hence resonance between upstream- and downstream-propagating waves. However, resonance is not excluded at the frequencies of the standing, zero-group-velocity (ZGV) GJWs, resonant by nature. The propagation of the waves radiated by the source is computed by solving the Euler equations. To deal with both upstream- and downstream-travelling GJWs (Towne et al. 2017), a high-subsonic Mach number of 0.95 is considered. The Strouhal number range is chosen to obtain GJWs belonging to the first two radial GJW axisymmetric modes. The source amplitude is small and the shear layer is very thick to prevent or limit the development of Kelvin-Helmholtz (KH) instability waves downstream of the source. For each source Strouhal number, the objective will be to ascertain whether GJWs travel in the jet flow, and if so, to determine their directions of propagation and their amplitudes inside and outside the flow. The properties of the GJWs will be explored by representing the levels of pressure fluctuations in the frequency-wavenumber space, where the dispersion curves predicted for GJWs using linear stability will also be plotted, as well as at given locations upstream and downstream of the source as a function of Strouhal number. The presence of tonallike peaks at specific frequencies, especially near the frequencies of the ZGV GJWs, in the present simplified flow configuration will especially be sought.

The paper is organised as follows. The jet flow conditions and the properties of the acoustic source in the flow, as well as the numerical parameters, are documented in § 2. The results are presented in § 3. Concluding remarks are given in § 4. Finally, pressure fields obtained for a source outside the flow are shown in the Appendix.

2. Parameters

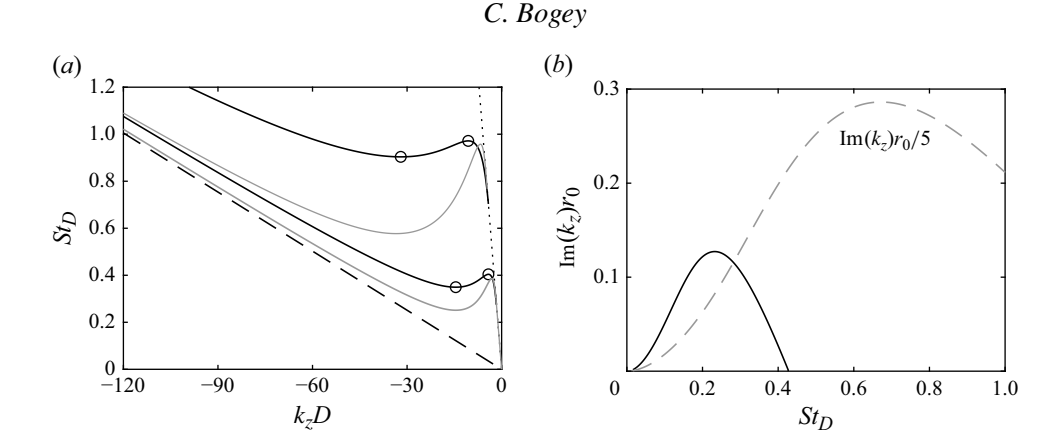
2.1. Jet flow and acoustic source

An isothermal round free jet at a Mach number $M = u_j/c_0 = 0.95$, in which a monopolar acoustic source is imposed on the centreline at the axial position z = 0, is considered. For simplicity, the jet consists of a cylindrical shear layer, surrounded by a medium at rest at temperature $T_0 = 293$ K and pressure $p_0 = 10^5$ Pa. Following Michalke (1984), the radial profile of the axial velocity u_z is defined by the hyperbolic-tangent profile

$$u_{z}(r) = \frac{u_{j}}{2} \left\{ 1 + \tanh \left[\frac{r_{0}}{4\delta_{\theta}} \left(\frac{r_{0}}{r} - \frac{r}{r_{0}} \right) \right] \right\}, \tag{2.1}$$

where $r_0 = D/2$ and δ_{θ} are the jet half-width and the shear-layer momentum thickness. The radial and azimuthal velocities are equal to zero, pressure is equal to p_0 and temperature is determined by a Crocco–Busemann relation. The momentum thickness is set to $\delta_{\theta} = 0.20r_0$. The large value of δ_{θ}/r_0 was chosen to avoid the presence of strong KH instability waves in the flow. Indeed, such waves might result in the formation and pairing of vortical structures, which could make the study of the GJWs difficult.

The acoustic source is placed on the jet centreline to generate axisymmetric GJWs. The GJW dispersion curves obtained for the azimuthal mode $n_{\theta} = 0$ for the present flow profile using linear-stability analysis are represented in figure 1(a) in the $k_z - St_D$ space. Due to the thick jet shear layer (Tam & Ahuja 1990; Edgington-Mitchell & Nogueira 2023; Maia *et al.* 2024), they differ significantly from the dispersion curves obtained for a vortex sheet, plotted for comparison. Despite this, as expected at a high-subsonic Mach number (Towne *et al.* 2017), the GJWs can have negative or positive group velocities $v_g = d\omega/dk_z$, thus propagating upstream or downstream. The GJWs can also have a zero group velocity at the stationary points of the dispersion curves, referred to as S_{min} and S_{max} when they correspond to a local minimum or maximum. These points, marked by circles,



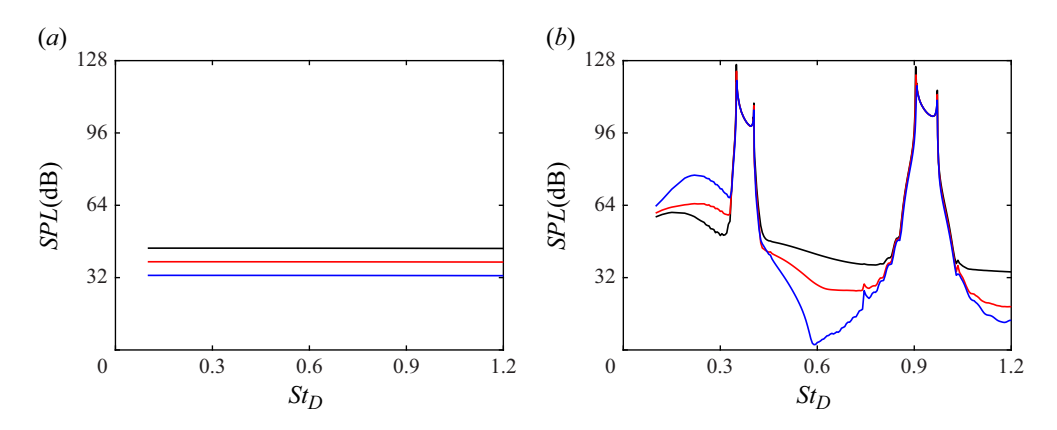


Figure 2. Variations with the Strouhal number of the sound pressure levels (SPL) obtained (a) without and (b) with flow at r = 0 and $z = 5r_0$, $z = 10r_0$ and $z = 20r_0$.

are at Strouhal numbers $St_D^{Smin,n_r=1} = 0.3493$, $St_D^{Smax,n_r=1} = 0.4041$, $St_D^{Smin,n_r=2} = 0.9037$ and $St_D^{Smax,n_r=2} = 0.9716$, where n_r is the radial mode number.

The acoustic source on the jet axis at z=0 has a Gaussian shape and a half-width of $3\Delta z(z=0)=3\Delta r(r=0)=0.06r_0$, where Δz and Δr are the axial and radial grid spacings. Its half-width is much smaller than the wavelength of the waves travelling at c_0 , the smallest one being equal to $1.75r_0$ when the source Strouhal number is maximum and equal to $St_D=1.2$, ensuring acoustical compactness. Its amplitude is very low to avoid appreciable nonlinear effects during the wave propagation and the generation of instability waves of high intensity. For illustration, the SPL obtained without flow at $5r_0$, $10r_0$ and $20r_0$ from the source are represented in figure 2(a) as a function of the source Strouhal number. At $5r_0$, for instance, they are approximately 42 dB, corresponding to root-mean-square (r.m.s.) values of pressure fluctuations of $p_{noflow}^{rrms}(5r_0) = 3.6 \times 10^{-3} \, \text{Pa}$.

The time evolution of the source amplitude is driven by a sinusoidal function of frequency $f_s = 1/T_s$, which is initially weighted by a half-Gaussian function increasing

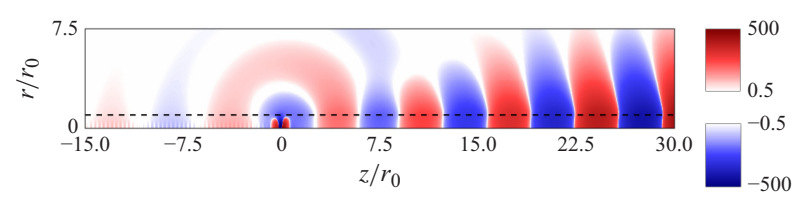


Figure 3. Pressure fluctuations obtained for $St_D = 0.23$; $- - r = r_0$. The levels are normalised by the r.m.s. value of pressure fluctuations obtained without flow at $5r_0$ from the source. They are represented using logarithmic scales.

between t = 0 and $t = 30T_s$. In the $n_{source} = 270$ simulations performed, the source Strouhal numbers are non-uniformly distributed between $St_D = 0.10$ and 1.20. They are clustered around the Strouhal numbers of the ZGV GJWs, around which the pressure amplitudes exhibit sharp variations and peak values. These variations appear, for example, in figure 2(b) showing the SPL obtained downstream of the source at $z = 5r_0$, $10r_0$ and $20r_0$ as a function of St_D . Levels between 100 and 125 dB are particularly found over two frequency ranges. They will be attributed to the presence of downstream-propagating GJWs belonging to the first and second radial axisymmetric GJW modes, respectively. Given the strong levels reached, the absence of significant nonlinear effects on the present results was verified by performing simulations using a ten times lower source amplitude at the first peak Strouhal number $St_D = 0.3495$ and at $St_D = 0.375$. The normalised solutions obtained using the two source amplitudes differ by less than 1 % in the first case and by less than 0.1 % in the second.

Finally, the amplification rates of the instability waves are calculated for the shear-layer profile using linear-stability analysis for the axisymmetric mode. They are represented in figure 1(b) as a function of St_D . Above $St_D=0.43$, they are negative, indicating that no instability waves should grow. For lower Strouhal numbers, they are weak. For comparison, they are approximately ten times weaker than those predicted for $\delta_\theta=0.05r_0$. As a result, it is most likely that instability waves develop, but that their amplitudes remain small. To check that, a snapshot of the pressure field obtained at the most unstable Strouhal number $St_D=0.23$ is provided in figure 3. KH instability waves are observed downstream of the source with amplitudes reaching $300 \times p_{noflow}^{\prime rms}(5r_0)$, corresponding to only 1 Pa, at $z=30r_0$, a position from which a sponge zone is implemented. Their entry in this zone does not seem to generate spurious acoustic waves travelling in the upstream direction. It can also be noted that no strong GJWs appear upstream.

2.2. Numerical methods and parameters

The computations are carried out by solving the Euler equations in cylindrical coordinates (r, θ, z) using the same numerical framework as in previous simulations of spatially developing (Bogey 2021, 2022a) and temporally developing (Bogey 2019; Bogey & Pineau 2019) round jets. The axis singularity is taken into account by the method of Mohseni & Colonius (2000). Fourth-order eleven-point centred finite differences are used for spatial discretisation, and a second-order six-stage Runge–Kutta algorithm is implemented for time integration. A twelfth-order centred filter is applied explicitly to the flow variables every time step to remove grid-to-grid oscillations. The radiation conditions of Tam & Dong (1996) are applied at the grid lateral boundaries. Periodic conditions are implemented at the inflow and outflow boundaries. Near these boundaries, sponge zones based on grid stretching and Laplacian filtering are built.

C. Bogey

2.3. Numerical parameters

In the axial direction, the mesh grid is symmetrical relative to z=0, and extends, excluding the 260-point inflow and outflow sponge zones, between $z=-30r_0$ and $z=30r_0$. In this region, the mesh spacing Δz is equal to $0.02r_0$, providing a wavenumber $k_z D=157$ for 4 points per wavelength (PPW). In the sponge zones, the mesh spacing is stretched at a rate of 3%, leading to grid boundaries located at $z=\pm 880r_0$. In the radial direction, the grid extends out to $r=25r_0$. The mesh spacing Δr is also equal to $0.02r_0$ between r=0 and $1.2r_0$. It then increases at a rate of 2.6% up $r=6.5r_0$, where $\Delta r=0.16r_0$, yielding $St_D=2.6$ for an acoustic wave with 5 PPW. The mesh spacing finally grows again between $r=16r_0$ and $21.6r_0$ to obtain $\Delta r=0.32r_0$ near the boundary. Thus, the grid contains $N_z=3519$ and $N_r=235$ points in the axial and radial directions. In the azimuthal direction, given that the flow and the sound waves are axisymmetric, only $N_\theta=2$ points are used and the derivatives are set to zero.

In the simulations with a source radiating in the ranges $0.38 \le St_D \le 0.4075$ and $0.90 \le St_D \le 0.975$, upstream- and downstream-propagating GJWs are found to both exist. In that case, spurious reflections might occur in the sponge zones and pollute the region $-30r_0 \le z \le 30r_0$ where the GJWs are studied. To avoid this, a larger grid, containing 4000 additionnal points in the central region where $\Delta z = 0.02r_0$, is used, to set the beginnings of the sponge zones at $z = \pm 70r_0$. The absence of GJWs reflected back in the sponge zones over $-30r_0 \le z \le 30r_0$ will be checked in the wavenumber–frequency representations of § 3.2.

The simulations are performed with an OpenMP-based in-house solver on single nodes containing 16–64 cores, using a time step $\Delta t = 0.65 \Delta r (r=0)/c_0$. After $t=30T_s$, they run during a time of $120r_0/(c_0-u_j)$ to allow the GJWs with a low group velocity to travel over large distances. Then, pressure is recorded during $100T_s$ in the azimuthal plane $\theta=0$ at every second point in the axial and radial directions between $z=\pm 30r_0$ and r=0 and s=0 and

3. Results

3.1. Pressure fields

Snapshots of pressure fluctuations $p-p_0$ obtained in (z,r) sections restricted to the near-source region for nine Strouhal numbers between $St_D=0.65$ and 1.03 are provided in figure 4. No KH instability waves appear downstream of the source, in agreement with linear-stability analysis. The source on the jet axis radiates waves that are transmitted as sound waves outside of the flow. These waves are of oval form due to convection and refraction effects and have amplitudes of the order $3 \times p_{noflow}^{\prime rms}(5r_0)$ close to the source, decreasing rapidly as they propagate as three-dimensional acoustic waves.

GJWs are visible upstream of the source in all cases, and downstream only in figure 4(e-h). When they exist, their amplitudes on the jet axis greatly exceed $30 \times p_{noflow}^{trms}(5r_0)$, and even nearly reach $3000 \times p_{noflow}^{trms}(5r_0)$ in figure 4(h). The amplitudes of the GJWs do not change with the distance to the source, which is consistent with the fact that they are neutral acoustic waves (Tam & Hu 1989) trapped into the jet due to total internal reflection (Nogueira *et al.* 2024). This is clearly shown by the SPL obtained on the jet axis at three downstream positions in figure 2(b). In this figure, the amplitudes at the peak frequencies slightly decrease with the distance to the source. This was found, by performing simulations over different time periods, to be due to the fact that, near these

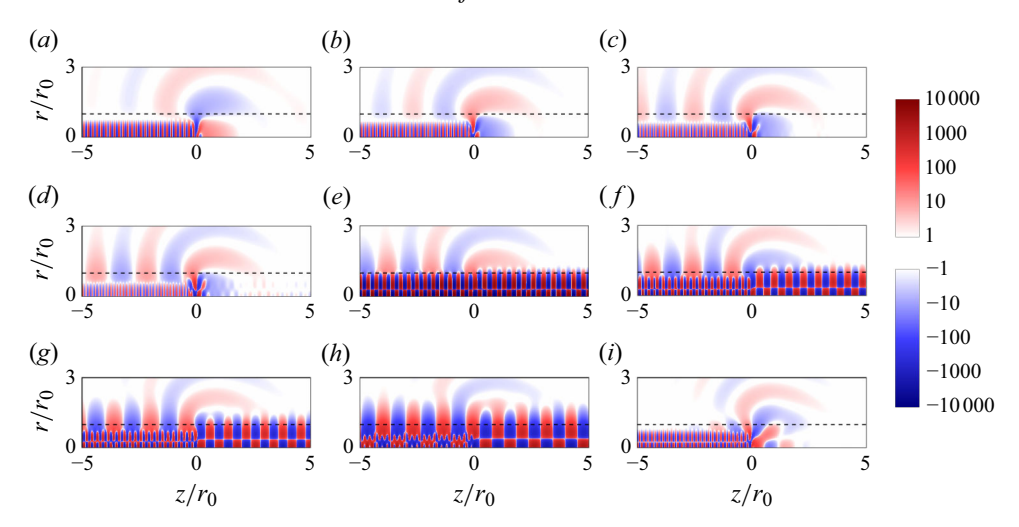


Figure 4. Pressure fluctuations obtained for Strouhal numbers (a) 0.65, (b) 0.74, (c) 0.805, (d) 0.855, (e) 0.905, (f) 0.93, (g) 0.95, (h) 0.97 and (i) 1.03; $---r = r_0$. The levels are normalised by the r.m.s. values of pressure fluctuations obtained without flow at $5r_0$ from the source. They are represented using logarithmic scales.

frequencies, corresponding to the frequencies of the ZGV GJWs, the wave energy travels at an extremely low velocity.

Regarding the characteristics of the GJWs, three cases can be distinguished depending on the Strouhal number range. First, for $0.65 \le St_D \le 0.855$ in figure 4(a-d), there are GJWs only upstream of the source. GJWs fully confined inside the jet with no node in their radial supports are seen. They are most likely duct-like GJWs of mode $n_r = 1$. Outside the jet, the levels are low but increase with the Strouhal number, suggesting the emergence of free-stream GJWs. Second, for $0.905 \le St_D \le 0.97$ in figure 4(e-h), there are GJWs both upstream and downstream of the source. A node appears in the radial supports of the waves, revealing the presence of GJWs of mode $n_r = 2$. Upstream of the source, the amplitudes at $r > r_0$ are significant and reach a peak value in figure 4(h) for $St_D = 0.97$. Downstream, the GJWs also leak out the jet shear layer. The leakage is quite weak at $St_D = 0.905$ but is much stronger as the Strouhal number rises. Thus, GJWs of free-stream nature are clearly found in all cases upstream but only near $St_D = 0.97$ downstream. Finally, for $St_D = 1.03$ in figure 4(i), there are, again, duct-like GJWs upstream of the source but no GJWs downstream as in figure 4(a-d). In this case, however, given the node in their radial support, the GJWs belong to the radial mode $n_r = 2$

For comparison, snapshots of pressure fluctuations obtained for an axisymmetric source placed outside the flow at z = 0 and $r = 2r_0$ at the same Strouhal numbers as in figure 4 are provided in the Appendix in figure 8. GJWs are also observed, but they appear to be essentially of free-stream nature and to have lower intensities compared with those in figure 4.

3.2. Levels of pressure fluctuations in the wavenumber-frequency space

To explain the GJW properties in this work, the pressure fluctuations recorded at r = 0 and $r = 2r_0$ between $z = -30r_0$ and $z = 30r_0$ are analysed in the $k_z - St_D$ space. The fluctuations obtained upstream and downstream of the source are treated separately to distinguish between the upstream- and the downstream-propagating waves. In practice,

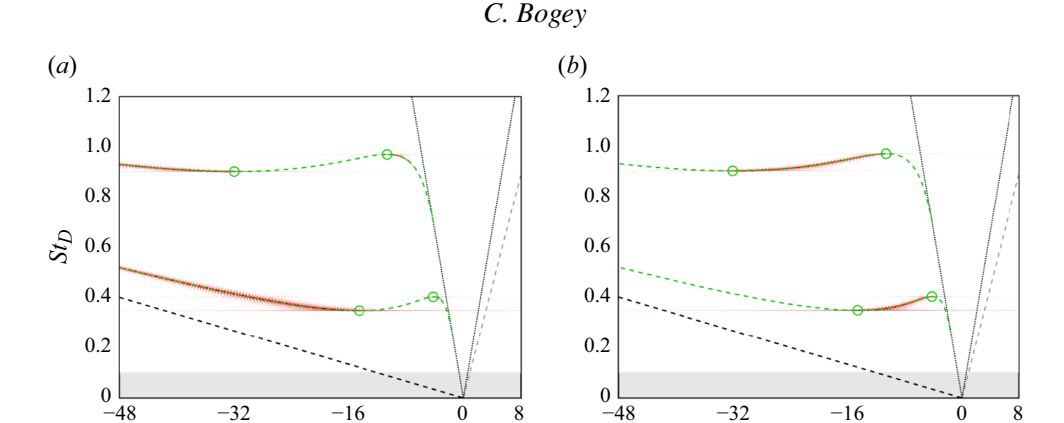


Figure 5. Representation in the wavenumber–frequency space of the levels of the pressure fluctuations obtained at r=0 (a) upstream and (b) downstream of the source; $--k_z=\omega/(u_j-c_0), \cdots k_z=\pm\omega/c_0, ---k_z=\omega/(0.7u_j); ---$ dispersion curves of the axisymmetric GJWs; $S_{min,n_r=1}$, $S_{max,n_r=1}$, $S_{min,n_r=2}$ and $S_{max,n_r=2}$, from bottom to top; no simulation in the grey zone. The levels in the white-to-red colour scale spread over 15 dB. They are the same in figures S(a) and S(b).

 k_zD

 k_zD

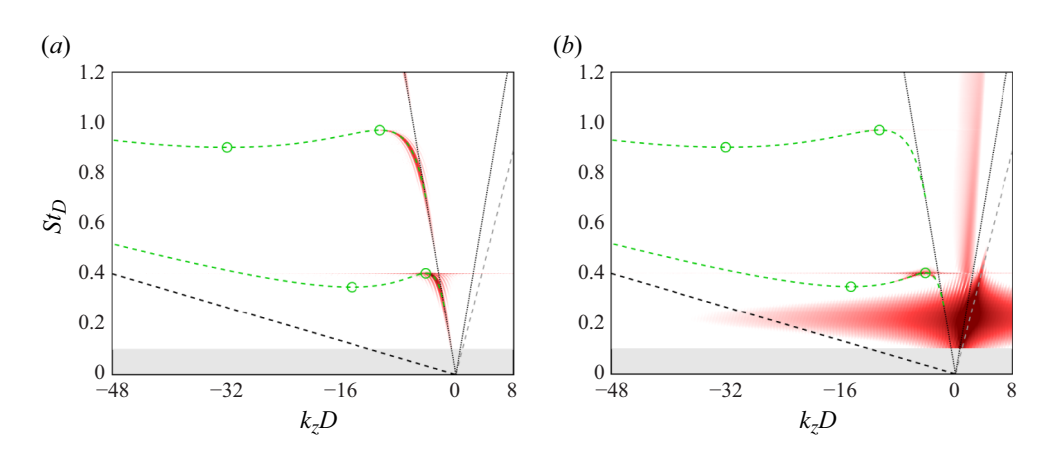


Figure 6. Representation in the wavenumber–frequency space of the levels of the pressure fluctuations obtained at $r = 2r_0$ (a) upstream and (b) downstream of the source; see caption of figure 5 for line and symbol types. Compared with figure 5, the colour-scale levels are 21 dB lower in figure 6(a) and 24 dB lower in figure 6(b).

for each simulation performed for a source Strouhal number St_{Di} ($i \in [1, n_{source}]$), a wavenumber–frequency transform is applied to the signals, providing spectra from which the $SPL_i(k_z)$ at St_{Di} are extracted. The levels $SPL_i(k_z)$ are then gathered in a matrix $[SPL_1; SPL_2; \ldots; SPL_{n_{source}}]$, yielding a spectrum that can be represented a function of k_z and $St_D = [St_{Di=1.n_{source}}]$.

The spectra thus determined are shown in figure 5 for the pressure fluctuations at r = 0 and in figure 6 for those at $r = 2r_0$. In both cases, the results obtained upstream and downstream of the source are given in the left and the right figures, respectively.

Downstream of the source, high levels emerge in the spectrum obtained at $r = 2r_0$ in figure 6(b) in a spot elongated along the convection line $k_z = \omega/(0.7u_j)$. They are restricted to the Strouhal number range where KH instability waves develop according to linear-stability analysis, and are strongest near the most unstable Strouhal number

 $St_D = 0.23$. Therefore, they are due to the instability waves growing in the jet shear layer. Significant levels also appear for positive wavenumbers above the sonic line $k_z = \omega/c_0$. They can be associated with the sound waves passing through the line $r = 2r_0$.

More importantly, high levels are found in all spectra for negative wavenumbers, organised along the GJW dispersion curves predicted using linear-stability analysis. It is worth noting here that the GJWs located upstream of the source in figures 5(a) and 6(a) all travel in the upstream direction, whereas the downstream GJWs in figures 5(b) and 6(b) all travel in the downstream direction. This implies that no GJWs are reflected back in the sponge zones, preventing the establishment of resonance between upstream- and downstream-propagating GJWs. Along the GJW dispersion curves, the levels vary quite differently inside and outside the jet flow.

On the jet axis, in figure 5, high levels are observed over the sections of the curves where GJWs are expected depending on their group velocity. The levels seem particularly strong near the stationary points S_{min} and S_{max} . Moreover, upstream of the source in figure 6(a), they are weaker when approaching the sonic line $k_z = -\omega/c_0$. Therefore, the amplitudes of the GJWs inside the jet decrease as the waves are less and less confined to the jet flow. This behaviour is in line with the finding of Nogueira *et al.* (2024) that the transmission coefficient of acoustic waves generated in a jet to the outside is maximum near the sonic line.

At $r = 2r_0$, in figure 6, the levels are significant only in the vicinity of the sonic line. This is due to the fact that far from the line, GJWs can only be duct-like GJWs entirely contained in the jet flow (Tam & Hu 1989; Towne *et al.* 2017). More surprisingly, the levels are highest near the points S_{max} . This is clearly the case for the first radial mode, in particular upstream of the source in figure 6(a). The latter result appears contradictory to the fact that, outside the jet, the amplitude of the pressure eigenfunctions predicted for the upstream-propagating GJWs, using a vortex-sheet model for instance, decreases when moving from the sonic line to the points S_{max} (Jordan *et al.* 2018; Bogey 2021). The eigenfunctions being normalised and all equal to 1 on the jet axis, the effects of this decrease are most likely counterbalanced by the high intensities of the GJWs near the stationary points mentioned above based on the results in figure 5.

3.3. SPL upstream and downstream of the source

To quantify the intensities of the GJWs and their variations with the frequency, which both cannot be easily determined using linear analysis, the differences ΔSPL between the SPL obtained with and without flow at $z=\pm 10r_0$, at r=0 and $r=2r_0$, are represented as a function of the source Strouhal number in figure 7(a) for $z=-10r_0$ and in figure 7(b) for $z=10r_0$. The frequencies of the stationary points S_{min} and S_{max} in the GJW dispersion curves are also shown. Except in the downstream spectra where a bump due to KH instability waves is observed at low Strouhal numbers, large positive values of ΔSPL indicate the presence of GJWs. Small positive values of ΔSPL may be due to GJWs of low intensity or to refraction effects. Lastly, negative values suggest that the acoustic waves radiated by the source do not generate GJWs, but are diverted away from the jet by refraction. This is the case, for instance, upstream at $St_D=0.1$ and downstream over $0.6 \le St_D \le 0.7$.

The values of $\triangle SPL$ obtained on the jet axis are plotted in black. Large values greater than 30 dB are found above $St_D^{Smin,n_r=1}$ for $z=-10r_0$ in figure 7(a) and over $St_D^{Smin,n_r=i} \le St_D \le St_D^{Smax,n_r=i}$ with i=1,2 for $z=10r_0$ in figure 7(b). According to the wavenumber–frequency representations of figure 5, they are due in the first case mostly to the upstream-propagating duct-like GJWs to left of the points S_{min} and,

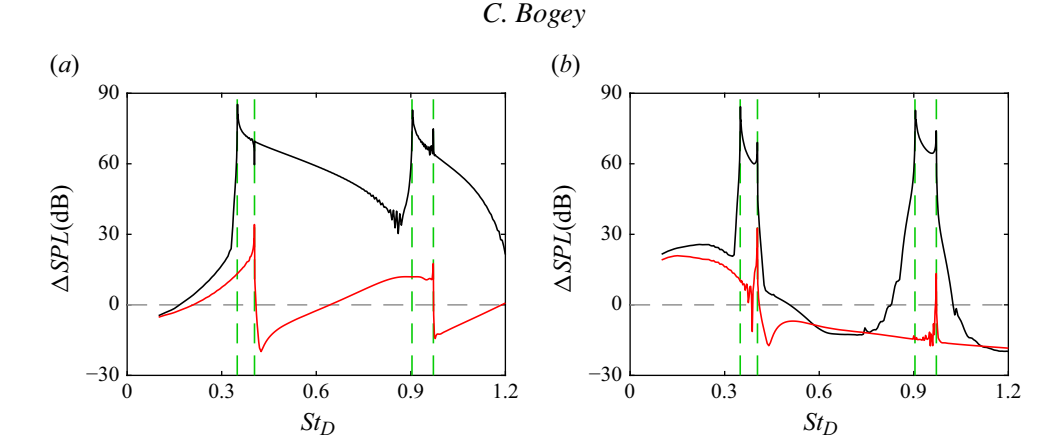


Figure 7. Variations with the Strouhal number of the difference between the SPL obtained with and without flow at (a) $z = -10r_0$ and (b) $z = 10r_0$, at r = 0 and $r = 2r_0$; $r = -10r_0$, $r = 2r_0$; $r = -10r_0$, $r = -10r_0$, $r = -10r_0$, at $r = -10r_0$, and $r = -10r_0$, at $r = -10r_0$, at $r = -10r_0$, at $r = -10r_0$, and $r = -10r_0$, and $r = -10r_0$, and $r = -10r_0$, at $r = -10r_0$, and $r = -10r_0$, and r = -

in the second, to the downstream-propagating GJWs between the points S_{min} and S_{max} . The intensities of the GJWs spectacularly depend on the frequency. Upstream of the source, the values of ΔSPL vary in a reverse sawtooth manner with the Strouhal number. Sharp rises of approximately 50 dB are observed at the cut-on Strouhal numbers $St_D^{Smin,n_r=1,2}$ of the upstream-propagating duct-like GJW modes, followed by gradual but sustained decreases. Downstream of the source, peaks emerge, nearly as tones, at the frequencies of the stationary points S_{min} and S_{max} . Given that in absolute value the group velocity of the upstream-propagating duct-like GJWs increases with the frequency above their cut-on Strouhal numbers, tending towards $c_0 - u_j$, and that the GJW group velocities are close to zero near the stationary points, these results suggest that the amplitudes of the GJWs are higher as their group velocities are lower. In the specific case of standing GJWs with ZGV, energy can be expected to only accumulate at the position of the source due to local resonance.

The values of $\triangle SPL$ obtained outside the jet, depicted in red, are quite different from those inside the jet. Upstream of the source, in figure 7(a), they fluctuate in a sawtooth manner with progressive increases up to peak values of 34 and 18 dB at $St_D^{Smax,n_r=1}$ and $St_D^{Smax,n_r=2}$, respectively, followed by sharp falls of 53 and 32 dB. Downstream, in figure 7(b), outside the frequency range of the KH instability waves, they are negative except near $St_D^{Smax,n_r=1,2}$, where peaks can be seen. The positive values of $\triangle SPL$ are due in the first case to the upstream-propagating free-stream GJWs between the sonic line and the points S_{max} in figure 6(a), and in the second to the downstream-propagating GJWs near the points S_{max} in figure 6(b). Again, the peaks near the frequencies of these points are tonal, supporting that the GJWs with a very low group velocity are very intense. As discussed above, this high intensity is most probably responsible for the emergence of the peaks observed upstream despite the fact that the GJWs around the points S_{max} are more confined inside the jet than those close to the sonic line.

Finally, it can be pointed out that the variations of the SPL obtained outside the jet upstream of the acoustic source with the frequency are very similar to the footprints left by the GJWs in the near-nozzle spectra of jets at comparable Mach numbers (Suzuki & Colonius 2006; Brès *et al.* 2018; Bogey 2021; Zaman *et al.* 2022).

4. Conclusion

The GJWs that can occur in a jet at M=0.95 are investigated by solving a problem of acoustic propagation, consisting of a source on the axis of a cylindrical shear layer radiating waves of low amplitude. This jet flow configuration was chosen to avoid reflections in the axial direction upstream or downstream of the source. When GJWs appear, their directions of propagation and radial supports vary with the source frequency. Their levels are illustrated in the wavenumber–frequency space. They are located along the dispersion curves of the axisymmetric GJW modes predicted using linear-stability analysis.

The amplitudes of the GJWs upstream and downstream of the source, inside and outside the jet, are quantified. When the waves exist, their amplitudes are very high. As the source frequency increases, they fluctuate in a sharp manner with discontinuities, and tonal-like peaks emerge near the frequencies of the standing GJWs with ZGV. In particular, outside the jet, upstream of the source, the peak levels at 10 jet radii from the source are up to 30 dB higher than those obtained without flow. Based on the present results, the GJW levels, measured on the jet axis, are found to depend on the degree of confinement of the waves inside the flow, as expected. They are weaker as the waves are less confined and tend to be sonic. They also appear to be stronger as the group velocities of the waves are lower, leading to the tonal peaks observed inside but also outside the jet. The latter point, as well as other ones such as the effects of the position of the source generating the acoustic waves and of the jet temperature, will be investigated in future studies.

The present study provides additional evidence that some properties of GJWs can be obtained by solving a problem of reflection and transmission of acoustic waves in a jet. It would be interesting to explain the mechanisms behind these properties by performing a linear-stability spatial analysis, similar to those reported in Huerre & Monkewitz (1990) for instance, considering the flow response to a harmonic source. The very high amplitudes of the GJWs near specific frequencies also explain why the feedback loops in resonant jets are most often closed by GJWs near the upper bounds of the allowable frequency ranges of the upstream-propagating free-stream GJWs. Finally, the tonal peaks at the frequencies of the ZGV GJWs suggest that such peaks can be obtained in the absence of axial resonance phenomena.

Acknowledgements. The author gratefully acknowledges E. De Staercke for performing linear-stability analyses from the jet flow profile. For the purpose of Open Access, a CC-BY public copyright licence has been applied by the author to the present document and will be applied to all subsequent versions up to the Author Accepted Manuscript arising from this submission.

Funding. This work was granted access to the HPC resources of PMCS2I of Ecole Centrale de Lyon and of CINES and IDRIS under the allocation 2024-2a0204 made by GENCI (Grand Equipement National de Calcul Intensif). It was performed within the framework of the LABEX CeLyA (ANR-10-LABX-0060) of Université de Lyon, within the program Investissements d'Avenir (ANR-16-IDEX-0005).

Declaration of interests. The author reports no conflict of interest.

Appendix. Pressure fields for a source outside the jet

Snapshots of pressure fluctuations obtained for an axisymmetric source located outside the jet at z=0 and $r=2r_0$ at Strouhal numbers between $St_D=0.65$ and 1.03 are given in figure 8. GJWs with a node in their radial supports, thus belonging to the mode $n_r=2$, appear. They differ significantly from those obtained for the source inside the jet at the same frequencies in figure 4. GJWs are visible upstream of the source only in figure 8(e-h) and downstream only in figure 8(h) for $St_D=0.97\simeq St_D^{Smax,n_r=2}$.

C. Bogey

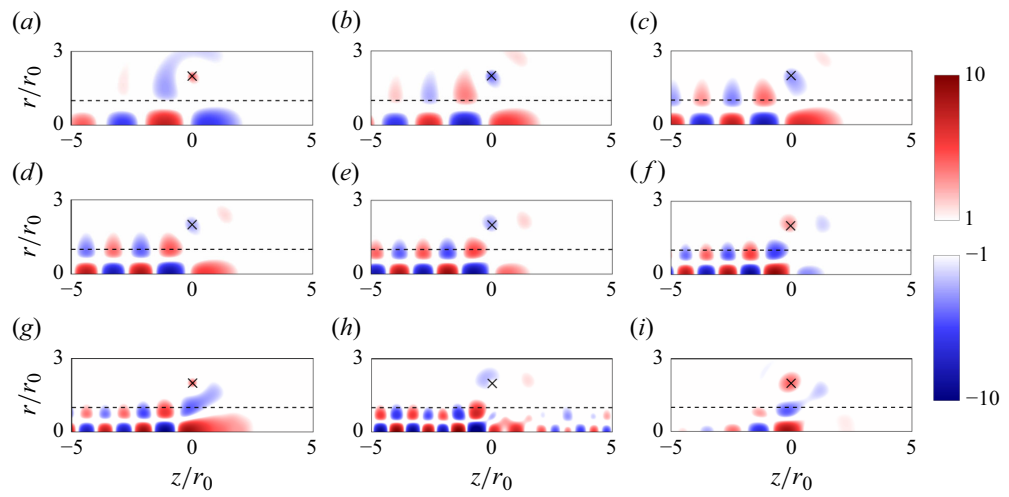


Figure 8. Pressure fluctuations obtained for an axisymmetric source at z=0 and $r=2r_0$ for Strouhal numbers (a) 0.65, (b) 0.74, (c) 0.805, (d) 0.855, (e) 0.905, (f) 0.93, (g) 0.95, (h) 0.97 and (i) 1.03; $---r=r_0$; × source position. The levels are normalised by the r.m.s. values of pressure fluctuations obtained without flow at r=0 and $z=-5r_0$ or $5r_0$. They are represented using logarithmic scales.

When they exist, the GJWs do not seem to be fully confined inside the flow. For instance, they do not resemble the duct-like GJWs observed in figure 4(a,i). In addition, their maximal amplitudes, reached for $St_D = 0.97$, do not exceed 10 times the r.m.s. values of pressure fluctuations obtained without flow on the jet axis at $z = -5r_0$ or $5r_0$. This suggests that GJWs can result from acoustic waves generated outside the jet, but that they are mostly of free-stream nature and have lower intensities than those resulting from waves inside the jet, especially near the frequencies of the standing GJWs.

REFERENCES

BOGEY, C. 2019 On noise generation in low Reynolds number temporal round jets at a Mach number of 0.9.
J. Fluid Mech. 859, 1022–1056.

BOGEY, C. 2021 Acoustic tones in the near-nozzle region of jets: characteristics and variations between Mach numbers 0.5 and 2. *J. Fluid Mech.* **921**, A3.

BOGEY, C. 2022a Interactions between upstream-propagating guided jet waves and shear-layer instability waves near the nozzle of subsonic and nearly ideally expanded supersonic free jets with laminar boundary layers. J. Fluid Mech. 949, A41.

BOGEY, C. 2022b Tones in the acoustic far field of jets in the upstream direction. AIAA J. 60 (4), 2397–2406.
BOGEY, C. 2024 Gain in efficiency of jet receptivity to acoustic disturbances with increasing nozzle-lip thickness. J. Fluid Mech. 997, A71.

BOGEY, C. & GOJON, R. 2017 Feedback loop and upwind-propagating waves in ideally-expanded supersonic impinging round jets. J. Fluid Mech. 823, 562–591.

BOGEY, C. & PINEAU, P. 2019 Potential-core closing of temporally developing jets at Mach numbers between 0.3 and 2: scaling and conditional averaging of flow and sound fields. *Phys. Rev. Fluids* 4 (12), 124601.

BRÈS, G.A., JORDAN, P., JAUNET, V., LE RALLIC, M., CAVALIERI, A.V.G., TOWNE, A., LELE, S.K., COLONIUS, T. & SCHMIDT, O.T. 2018 Importance of the nozzle-exit boundary-layer state in subsonic turbulent jets. J. Fluid Mech. 851, 83–124.

EDGINGTON-MITCHELL, D. 2019 Aeroacoustic resonance and self-excitation in screeching and impinging supersonic jets – a review. *Intl J. Aeroacoust.* 18 (2–3), 118–188.

EDGINGTON-MITCHELL, D., JAUNET, V., JORDAN, P., TOWNE, A., SORIA, J. & HONNERY, D. 2018 Upstream-travelling acoustic jet modes as a closure mechanism for screech. *J. Fluid Mech.* 855, R1.

EDGINGTON-MITCHELL, D. & NOGUEIRA, P.A.S. 2023 The guided-jet mode in compressible jets. *Tech. Rep.* 2023-3647. AIAA Paper.

- GOJON, R., BOGEY, C. & MIHAESCU, M. 2018 Oscillation modes in screeching jets. AIAA J. 56 (7), 2918–2924.
- HUERRE, P. & MONKEWITZ, P.A. 1990 Local and global instabilities in spatially developing flows. Annu. Rev. Fluid Mech. 22, 473–537.
- JORDAN, P., JAUNET, V., TOWNE, A., CAVALIERI, A.V.G., COLONIUS, T., SCHMIDT, O. & AGARWAL, A. 2018 Jet–flap interaction tones. *J. Fluid Mech.* 853, 333–358.
- MAIA, I.A., FIORE, M. & GOJON, R. 2024 Tones and upstream-traveling waves in ideally expanded round impinging jets. *Phys. Rev. Fluids* **9** (8), 083904.
- MARTINI, E., CAVALIERI, A.V.G. & JORDAN, P. 2019 Acoustic modes in jet and wake stability. J. Fluid Mech. 867, 804–834.
- MICHALKE, A. 1984 Survey on jet instability theory. Prog. Aerosp. Sci. 21, 159–199.
- MOHSENI, K. & COLONIUS, T. 2000 Numerical treatment of polar coordinate singularities. *J. Comput. Phys.* **157** (2), 787–795.
- NOGUEIRA, P. & EDGINGTON-MITCHELL, D. 2021 Investigation of supersonic twin-jet coupling using spatial linear stability analysis. *J. Fluid Mech.* **918**, A38.
- NOGUEIRA, P.A.S., CAVALIERI, A.V.G., MARTINI, E., TOWNE, A., JORDAN, P. & EDGINGTON-MITCHELL, D. 2024 Guided-jet waves. *J. Fluid Mech.* 999, A47.
- SCHMIDT, O., TOWNE, A., COLONIUS, T., CAVALIERI, A.V.G., JORDAN, P. & BRÈS, G.A. 2017 Wavepackets and trapped acoustic modes in a turbulent jet: coherent structure eduction and global stability. *J. Fluid Mech.* 825, 1153–1181.
- SUZUKI, T. & COLONIUS, T. 2006 Instability waves in a subsonic round jet detected using a near-field phased microphone array. *J. Fluid Mech.* **565**, 197–226.
- TAM, C.K.W. & AHUJA, K.K. 1990 Theoretical model of discrete tone generation by impinging jets. J. Fluid Mech. 214, 67–87.
- TAM, C.K.W. & CHANDRAMOULI, S. 2020 Jet-plate interaction tones relevant to over-the-wing engine mount concept. J. Sound Vib. 486, 115378.
- TAM, C.K.W. & DONG, Z. 1996 Radiation and outflow boundary conditions for direct computation of acoustic and flow disturbances in a nonuniform mean flow. *J. Comput. Acous.* 4 (2), 175–201.
- TAM, C.K.W. & Hu, F.Q. 1989 On the three families of instability waves of high-speed jets. J. Fluid Mech. 201, 447–483.
- TOWNE, A., CAVALIERI, A.V.G., JORDAN, P., COLONIUS, T., SCHMIDT, O., JAUNET, V. & BRÈS, G.A. 2017 Acoustic resonance in the potential core of subsonic jets. *J. Fluid Mech.* **825**, 1113–1152.
- VARÉ, M. & BOGEY, C. 2022 Generation of acoustic tones in round jets at a Mach number of 0.9 impinging on a plate with and without a hole. *J. Fluid Mech.* **936**, A16.
- ZAMAN, K.B.M.Q., FAGAN, A.F., BRIDGES, J.E. & BROWN, C.A. 2015 An experimental investigation of resonant interaction of a rectangular jet with a flat plate. *J. Fluid Mech.* 779, 751–775.
- ZAMAN, K.B.M.Q., FAGAN, A.F. & UPADHYAY, P. 2022 Pressure fluctuations due to trapped waves in the initial region of compressible jets. *J. Fluid Mech.* 931, A30.
- ZAMAN, K.B.M.Q., FAGAN, A.F. & UPADHYAY, P. 2023 Pressure fluctuation spectral peaks due to 'guided waves' in regions upstream of the jet exit. *Tech. Rep.* 2023–3649. AIAA Paper.